Lasers in Surgery and Medicine 53:1096–1104 (2021)

Incident Fluence Analysis for 755-nm Picosecond Laser Treatment of Pigmented Skin Lesions Based on Threshold Fluences for Melanosome Disruption

Yu Shimojo, MS,[1*] Takahiro Nishimura, PhD,[1*] Hisanao Hazama, PhD,[1] Nobuhisa Ito, MD, PhD,[2] and Kunio Awazu, PhD, MD[1,2,3]

[1]*Graduate School of Engineering, Osaka University, Yamadaoka 2-1, Suita, Osaka, 565-0871, Japan*

[2]*Global Center for Medical Engineering and Informatics, Osaka University, Yamadaoka 2-2, Suita, Osaka, 565-0871, Japan*

[3]*Graduate School of Frontier Biosciences, Osaka University, Yamadaoka 1-3, Suita, Osaka, 565-0871, Japan*

Background and Objectives: In this study, the threshold fluences for disrupting the melanosomes for pigmented skin lesion treatment were determined using a 755-nm picosecond laser for clinical use. Based on the melanosome disruption thresholds, incident fluences corresponding to the target lesion depths were evaluated *in silico* for different laser spot sizes.

Study Design/Materials and Methods: Melanosome samples were isolated from porcine eyes as alternative samples for human cutaneous melanosomes. The isolated melanosomes were exposed to 755-nm picosecond laser pulses to measure the mean particle sizes by dynamic light scattering and confirm their disruption by scanning electron microscopy. The threshold fluences were statistically determined from the relationships between the irradiated fluences and the mean particle sizes. Incident fluences of picosecond laser pulses for the disruption of melanosomes located at different depths in skin tissue were calculated through a light transport simulation using the obtained thresholds.

Results: The threshold fluences of 550- and 750-picosecond laser pulses were determined to be 2.19 and 2.49 J/cm^2, respectively. The numerical simulation indicated that appropriate incident fluences of picosecond laser pulses differ depending on the depth distribution of the melanosomes in the skin tissue, and large spot sizes are desirable for disrupting the melanosomes more deeply located within the skin tissue.

Conclusion: The threshold fluences of picosecond laser pulses for melanosome disruption were determined. The incident fluence analysis based on the thresholds for melanosome disruption provides valuable information for the selection of irradiation endpoints for picosecond laser treatment of pigmented skin lesions. Lasers Surg. Med. © 2021 The Authors. *Lasers in Surgery and Medicine* published by Wiley Periodicals LLC

Key words: picosecond laser pulse; threshold fluence; melanosome disruption; pigmented lesions; skin tissue; irradiation condition; light transport simulation

INTRODUCTION

The therapeutic application of picosecond lasers provides highly efficacious and minimally invasive treatments for pigmented skin lesions through selective photothermolysis [1]. Picosecond laser pulses with a much shorter width than the thermal relaxation time of the melanosomes (approximately 0.5–1 μs) can confine heat and increase the temperature owing to the high peak-power density [2]. This process induces selective melanosome disruption, resulting in treatment effects [3,4]. As picosecond laser pulses propagate in skin tissue, the incident fluence is attenuated by the epidermis and dermis through their high-scattering nature [5,6]. Because skin tissues affected by pigmented lesions have different depth distributions of melanosomes [7-9], the extent to which the incident fluence reaches the target lesions depends on their depth. Picosecond laser-tissue interaction analysis based on optical attenuation and threshold fluence for melanosome disruption enables the estimation of the laser fluence reaching lesions at a given skin-tissue depth. Thus, the appropriate irradiation parameters for picosecond laser treatment of pigmented skin lesions can be determined.

Conflict of Interest Disclosures: All authors have completed and submitted the ICMJE Form for Disclosure of Potential Conflicts of Interest and none were reported.

Contract grant sponsor: Japan Society for the Promotion of Science KAKENHI; Contract grant number: 19K22966.

[*]**Correspondence to**: Yu Shimojo, Graduate School of Engineering, Osaka University, Yamadaoka 2-1, Suita, Osaka 565-0871, Japan.

E-mail: shimojoy@mb.see.eng.osaka-u.ac.jp

Takahiro Nishimura, Graduate School of Engineering, Osaka University, Yamadaoka 2-1, Suita, Osaka 565-0871, Japan.

E-mail: nishimura-t@see.eng.osaka-u.ac.jp

Accepted 1 February 2021

Published online 19 February 2021 in Wiley Online Library (wileyonlinelibrary.com).

DOI 10.1002/lsm.23391

Threshold fluences of short laser pulses with various widths have been investigated for selective melanosome response [10-16], and the threshold fluences of femtosecond-to-microsecond laser pulses for melanosome disruption in laser skin treatment have been reported [10,11]. Such studies visually observed the disruption through the grossly apparent immediate whitening response of the skin surface from increased optical scattering. The incident fluences were affected by optical attenuation in the skin before reaching the target melanosomes. Melanosome disruption from the net threshold fluences was not shown. Experimental analyses of picosecond-to-microsecond laser pulses in selective retina treatment have also been conducted using melanosomes isolated from porcine and bovine eyes [12-16]. However, these analyses investigated the threshold fluences for the microbubble formation around the melanosomes, overstretching the retinal pigment epithelium (RPE) cell membrane [17]. These reported values are inapplicable to melanosome disruption. A detailed investigation into melanosome disruption by picosecond laser pulses is required to evaluate the picosecond laser irradiation conditions for pigmented skin lesion treatment.

Incident fluence analysis for picosecond laser treatment of pigmented skin lesions based on threshold fluences for melanosome disruption is discussed in this paper. Melanosome samples isolated from porcine eyes were exposed to 755-nm picosecond laser pulses for therapeutic use to measure the mean particle sizes irradiated with varying fluences by dynamic light scattering (DLS) and confirm their disruption by scanning electron microscopy (SEM). The threshold fluences were determined from the irradiated fluences and the mean particle sizes. A Monte Carlo simulation of light transport in tissue was conducted to calculate the incident fluences of picosecond laser pulses for the disruption of melanosomes located at different skin-tissue depths. Because a Monte Carlo simulation can produce a light distribution of skin tissue with high accuracy [18-21], a threshold-based incident fluence analysis allows for a prediction of appropriate irradiation conditions for picosecond laser pulses to reach pigmented skin lesions with minimal damage to the surrounding tissue.

MATERIALS AND METHODS

Determination of Threshold Fluences of Picosecond Laser Pulses for Melanosome Disruption

Sample preparation of melanosome suspensions. Melanosomes isolated from the RPE of fresh porcine eyes (purchased from Tokyo Shibaura Zouki, Tokyo, Japan) were prepared as alternative samples for human cutaneous melanosomes [12]. They were dissected, and the lens and vitreous removed. Subsequently, they were immersed in distilled water briefly, and the neural retina was peeled off. The RPE cells were extracted using a toothbrush and suspended in distilled water. The suspensions were purified using a glass microfiber filter with a 2.7-μm pore size (1823-090; Whatman, Buckinghamshire, UK) to collect the melanosomes released from the RPE cells. Distilled water was added to the purified suspensions such that the samples had an optical density of about 0.05 at a wavelength of 755 nm when the sample thickness was 1 cm, thus providing laser energy from the sample surface to the bottom. Because no aggregation of the melanosomes was observed using an inverted laboratory microscope (Leica DM IRB; Leica, Wetzlar, Germany), the effects of the interaction between the individual melanosomes were discounted. The irradiation samples were stored at 4°C until use.

Laser system and irradiation setup. A 755-nm picosecond alexandrite laser for therapeutic use (PicoSure; Cynosure, Westford, MA) was employed. The irradiation conditions are listed in Table 1. The irradiation parameters were based on the nominal values specified on the system operation manual (PicoSure Operator Manual). Various fluences were used to determine the threshold. The fluence was dependent on the spot size; the larger the spot size, the lower the fluence, for example, 2.0 mm at 5.25 J/cm^2 for 550 picoseconds. The variance in the measured power density over an incident beam obtained from the beam profile data was within the range of −20% to +30% from the averaged value. The samples that were to be irradiated were added to Petri dishes to a 1-cm height (179830; Thermo Fisher Scientific, Waltham, MA), under which a sheet of black flocked paper (BFP1; Thorlabs,

TABLE 1. Irradiation Conditions for Picosecond Alexandrite Laser Based on the Nominal Values Specified on the PicoSure Operator Manual

	Picosecond alexandrite laser	
Wavelength (nm)	755	
Pulse width (ps)	550	750
Spot size (mm)	2.0, 2.6, 2.8, 2.9, 3.0, 3.1, 3.2, 3.4, 3.6, 4.0, 4.4, 4.8	2.2, 2.6, 2.8, 2.9, 3.0, 3.1, 3.2, 3.3, 3.4, 3.5, 3.6, 4.0, 5.0
Fluence (J/cm^2)	0.91, 1.09, 1.31, 1.62, 2.04, 2.19, 2.33, 2.50, 2.68, 3.11, 5.25	1.02, 1.59, 1.96, 2.08, 2.20, 2.34, 2.49, 2.65, 2.83, 3.03, 3.25, 3.77, 5.26
Repetition rate (Hz)	1	
Output stability of fluence (%)	±20	
Variance of spot size (%)	±10	

Newton, NJ) was placed to prevent backscattering. The handpiece tip was fixed on the sample surface to maintain a constant distance between the surface and the irradiation port. The laser light was irradiated with the beam divergence (full angle) of 11 to 77 mrad. The optical axis was adjusted to be perpendicular to the sample surface. During the irradiation, the samples were moved with a motorized linear translation stage (SGSP20-20(XY); Sigmakoki, Tokyo, Japan) at a speed of the laser spot sizes per second in such a way that the entire surface was irradiated without the overlapping of already irradiated spots. The temperature of the samples was maintained at 37°C during irradiation using a digital temperature controller (TS-P; As One, Osaka, Japan) and a silicon rubber heater (SAM0310; Sakaguchi E.H VOC, Tokyo, Japan).

Measurement of mean melanosome sizes for determination of threshold fluences. In determining the threshold fluences, melanosome disruption was measured by comparing the mean particle sizes of unirradiated melanosomes and melanosomes irradiated with picosecond laser pulses. The measurements were carried out with a particle size analyzer (Zetasizer Nano ZS; Malvern, Worcestershire, UK) using DLS, incorporating noninvasive backscatter optics. This technique measures the time-dependent fluctuations in the intensity of scattered light occurring from Brownian motion [22]. The measurement results do not depend on the number of particles [23]. The irradiated samples were placed into disposable cells (BRA759116; As One). The refractive indexes of the melanosomes and distilled water were 1.65 and 1.33, respectively [24]. Each sample was measured three times, and the values averaged.

Morphological observation of melanosomes irradiated using picosecond laser pulses. The morphologies of unirradiated melanosomes and melanosomes irradiated with picosecond laser pulses were observed using a SEM (JCM-5700; JEOL, Tokyo, Japan) to confirm their disruption. Laser irradiation was applied at a pulse width of 550 picoseconds and a fluence of $5.25\,\mathrm{J/cm^2}$ because it was inferred that melanosomes could be disrupted and clearly observed under this irradiation condition from Figure 2. The melanosomes were dried and platinum-coated to 5 nm using an ion-sputtering system (E-1010; Hitachi, Tokyo, Japan) to increase the electrical conductivity. The long axes of the melanosomes in the scanning electron micrographs were measured using an image processing software, ImageJ (National Institute of Health, Bethesda, MD).

Statistical analysis. A two-tailed unpaired Student's *t*-test determined a significant difference in the mean particle sizes between unirradiated melanosomes and melanosomes irradiated with picosecond laser pulses, with a probability value of $P < 0.01$ indicating statistical significance.

Incident Fluence Analysis of Picosecond Laser Pulses for Melanosome Disruption in Skin Tissue

Theory on incident fluence analysis of picosecond laser pulses. Pigmented lesions, such as solar lentigines, nevus of Ota, acquired dermal melanocytosis, and ectopic Mongolian spots were distributed at different depths in the epidermis/dermis [7-9]. Because an incident laser pulse is attenuated by the epidermis and dermis owing to their high scattering, incident fluences for picosecond laser irradiation to the target lesions located at different depths can vary to produce selective photothermolysis. The incident fluence $F(\mathbf{r})$ ($\mathrm{J/cm^2}$) delivering the threshold fluence into the target melanosomes at position $\mathbf{r}$ is expressed as

$$F(\mathbf{r}) \cdot A \cdot I(\mathbf{r}) \geq H_{\mathrm{th}} \tag{1}$$

where A ($\mathrm{cm^2}$) is the laser spot area, $I(\mathbf{r})$ ($1/\mathrm{cm^2}$) is the relative fluence distribution at position $\mathbf{r}$ produced using Monte Carlo simulations, and H_{th} ($\mathrm{J/cm^2}$) is the threshold fluence of picosecond laser pulses for determining melanosome disruption. Here, $A \cdot I(\mathbf{r})$ in Equation (1) was defined as the light-propagation efficiency of skin tissue from the irradiated surface to position $\mathbf{r}$, $\alpha(\mathbf{r})$ (unitless quantity) because it indicates the light distribution of skin tissue when a unit of laser fluence is incident over the spot area A. Substituting $\alpha(\mathbf{r})$ to Equation (1), the following equation was obtained:

$$F(\mathbf{r}) \cdot \alpha(\mathbf{r}) \geq H_{\mathrm{th}} \tag{2}$$

The incident fluences $F(\mathbf{r})$ were calculated using this equation.

Monte Carlo simulation of light transport in skin tissue. A 3D Monte Carlo code, mcxyz, was employed to calculate the relative fluence distribution when skin tissue was irradiated with a 755-nm picosecond laser [25]. This light transport model is a computer simulation of the light distribution within complex tissues consisting of different types, each with its own optical properties. In this simulation, a rectangular wave pulse with a uniform square spot shape was assumed to be vertically irradiated at the center of the skin surface [26,27]. The largest absorption coefficient in the skin model was $0.49\,\mathrm{mm^{-1}}$ (Table 2) and the maximum power density was calculated as $9.6 \times 10^9\,\mathrm{W/cm^2}$ by dividing fluence by pulse width [28,29]. The maximum power density is two orders of magnitude less than the threshold for the nonlinear excitation condition of the skin tissue [30]. The nonlinear absorption induced through picosecond laser irradiation can be negligible. The simulation was carried out for 180 million photons to achieve sufficient relative light distributions of skin tissue. Figure 1 shows the numerical model of human skin tissue geometry to calculate the light distributions [5,31]. This numerical model comprises the epidermis, dermis, subcutaneous fat layers, and three different sized blood vessels in the dermis layer and the model was constructed using $500 \times 500 \times 400$ cubicle

TABLE 2. Absorption μ_a and Reduced Scattering μ_s' Coefficients and Anisotropy Factor g of Asian Human Epidermis, Dermis, Subcutaneous Fat, and Blood at a Wavelength of 755 nm

	μ_a (mm^{-1})	μ_s' (mm^{-1})	g (–)
Epidermis	0.49 ± 0.19	4.28 ± 1.04	0.9
Dermis	0.05 ± 0.01	2.20 ± 0.43	0.9
Subcutaneous fat	0.04 ± 0.02	1.43 ± 0.22	0.9
Blood	0.32	1.68	0.9

μ_a and μ_s' of each tissue layer are expressed as mean ± standard deviation.

voxels. The size of each voxel was 10 μm × 10 μm × 10 μm. The depth direction of the model was set as the z-axis. The skin surface was set at $z = 0$ mm. The center of the model on the xy-plane was set at $(x, y) = (0\text{ mm}, 0\text{ mm})$. A melanin layer mimicking pigmented skin lesions was absent in the model. This numerical simulation calculated the incident fluences to deliver the threshold on the surface of a single melanosome located at a given depth within the skin tissue, assuming that it absorbs the laser light in the same way as the melanosome in water. Absorption μ_a and reduced scattering μ_s' coefficients, and anisotropy factor g for Asian human skin tissues at a wavelength of 755 nm were used in the skin model, as listed in Table 2 [5]. Melanin in the normal epidermis was simulated to be uniformly distributed in the epidermis layer of the skin model. The effect of optical absorption by the normal melanin was included in the μ_a of the epidermis. The blood oxygen saturation was 96%.

RESULTS

Determination of Threshold Fluences through DLS Analysis and SEM Observation of Melanosomes

The mean particle sizes of unirradiated melanosomes and melanosomes irradiated with picosecond laser pulses were statistically compared to determine the threshold fluences for melanosome disruption. Figure 2 shows the mean particle sizes of melanosomes exposed to 550- and 750-picosecond laser pulses with varying fluences. The mean particle sizes decreased with increasing irradiated fluence. The mean particle sizes of unirradiated melanosomes in Figure 2a were slightly larger than those in Figure 2b, owing to individual differences in the melanosome sizes. A statistical comparison indicated that the mean particle sizes significantly changed when 550- and 750-picosecond laser pulses were irradiated at or above 2.19 and 2.49 J/cm^2, respectively. The morphologies of unirradiated melanosomes and melanosomes irradiated with picosecond laser pulses were then observed with SEM to confirm melanosome disruption when the mean particle sizes changed significantly (Fig. 3). Although the unirradiated melanosomes retained their native shape (Fig. 3(i)), the smooth surface structures were broken in the irradiated melanosomes (Fig. 3(ii)). The lengths of the unirradiated and irradiated melanosomes were 1.6 ± 0.3 and 1.3 μm, respectively, and the sizes of the disrupted melanosomes decreased, having consistency with the results of the DLS analysis. Therefore, the DLS analysis and SEM observation resulted in determining the threshold fluences for melanosome disruption for 550- and 750-picosecond laser pulses as 2.19 and 2.49 J/cm^2, respectively.

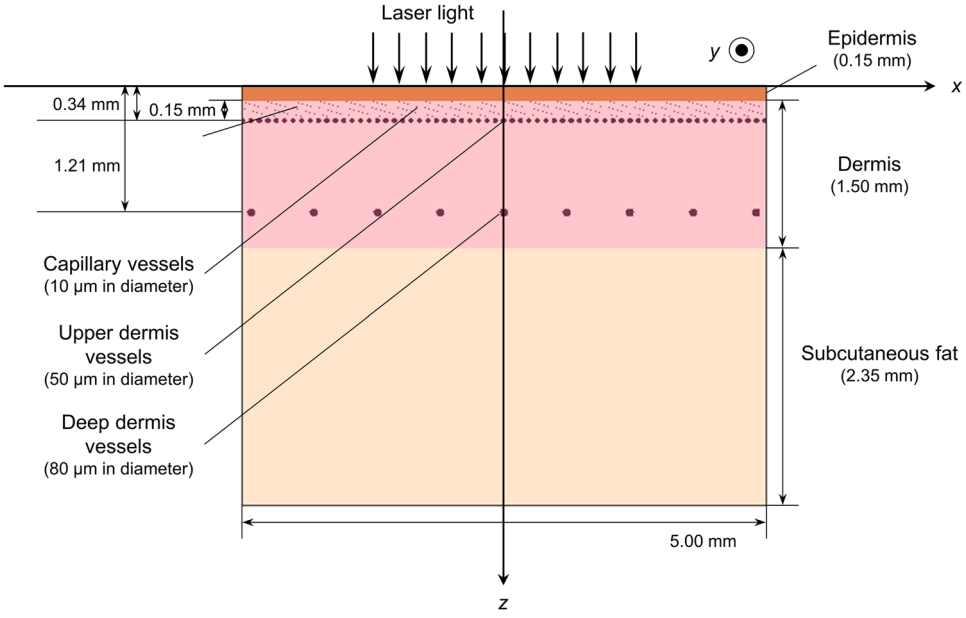

Fig. 1. Numerical model of human skin geometry consisting of the epidermis, dermis, subcutaneous fat, and three different sized blood vessels (capillary vessels, upper dermis vessels, and deep dermis vessels).

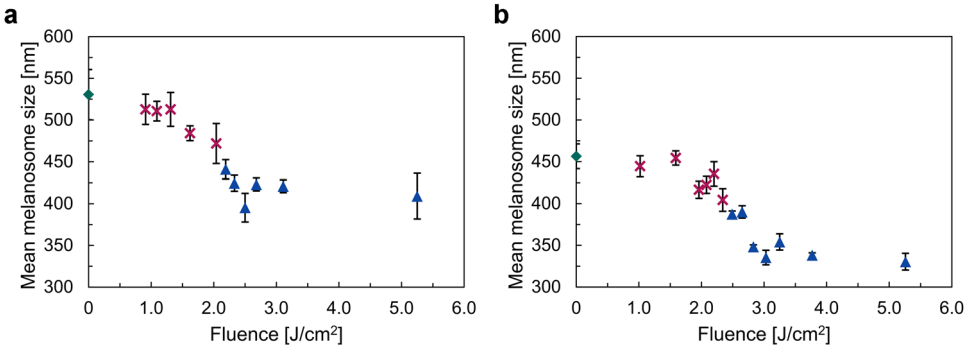

Fig. 2. Mean melanosome sizes after (**a**) 550- and (**b**) 750-picosecond laser pulse irradiations with varying irradiation fluences measured using a particle size analyzer ($n = 3$). Error bars represent the standard deviation (SD) of the mean melanosome sizes. The differences in the mean particle sizes between irradiated (crosses and triangles) and unirradiated (diamonds) melanosomes were statistically evaluated. Despite no significant differences in the crosses, there are significant differences in the triangles ($P < 0.01$). The threshold fluences of 550- and 750-picosecond laser pulses disrupting the melanosomes were determined as 2.19 and 2.49 J/cm^2, respectively.

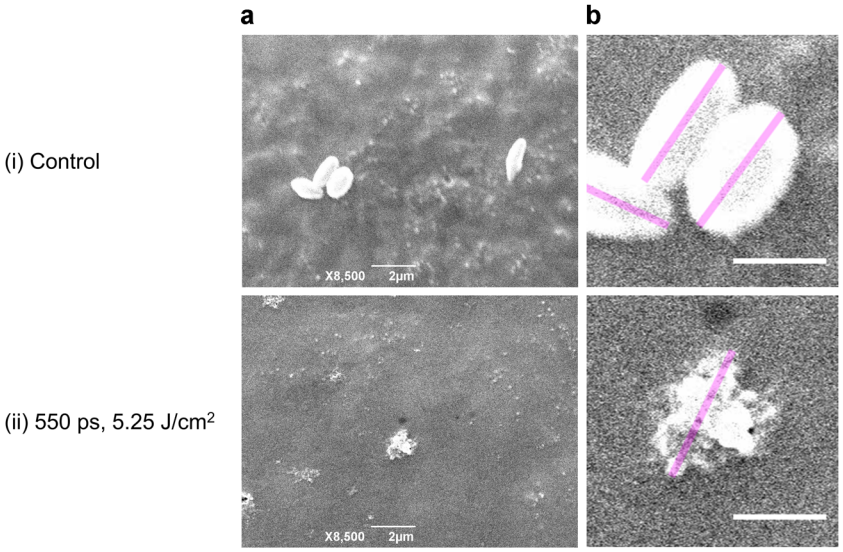

Fig. 3. (**a**) Melanosome disruption was confirmed based on comparison of scanning electron micrographs of (**i**) unirradiated melanosomes and (**ii**) melanosomes irradiated using a picosecond laser. The 755-nm picosecond laser pulses were irradiated at a pulse width of 550 picoseconds and a fluence of 5.25 J/cm^2. (**b**) The melanosomes were shown with greater magnification. The long axes of the melanosomes shown as the pink lines were measured using the ImageJ. Scale bars in (**a**) and (**b**) indicate 2 and 1 μm, respectively.

Incident Fluences of Picosecond Laser Pulses for Melanosome Disruption in Skin Tissue

The incident fluences for the disruption of melanosomes distributed at different depths in skin tissue were obtained using Equation (2). Figure 4 shows the light-propagation efficiencies α produced through Monte Carlo simulations at spot sizes of 2, 3, and 4 mm. The light-propagation efficiencies tend to decrease with increasing depth in the skin tissue. The maximum and minimum dispersions of α were estimated using the SD of μ_a and μ_s' of each tissue layer, derived from individual and body-site differences [5]. The maximum α was obtained from the minimum μ_a and μ_s' (mean – 1 SD), whereas the minimum α was obtained from the maximum μ_a and μ_s' (mean + 1 SD). The laser pulse entering the skin tissue propagates radially (Fig. 4(i)). The light-propagation efficiencies increase near the dermal-epidermal junction owing to the backscattering (Fig. 4(ii)).

Figure 5 shows the incident fluences of 550- and 750-picosecond laser pulses for the disruption of melanosomes distributed at different depths in skin tissue when the spot size is 2, 3, and 4 mm. The incident fluences increase with increasing depth of the target melanosomes. The deviation of the incident fluences increases as the target

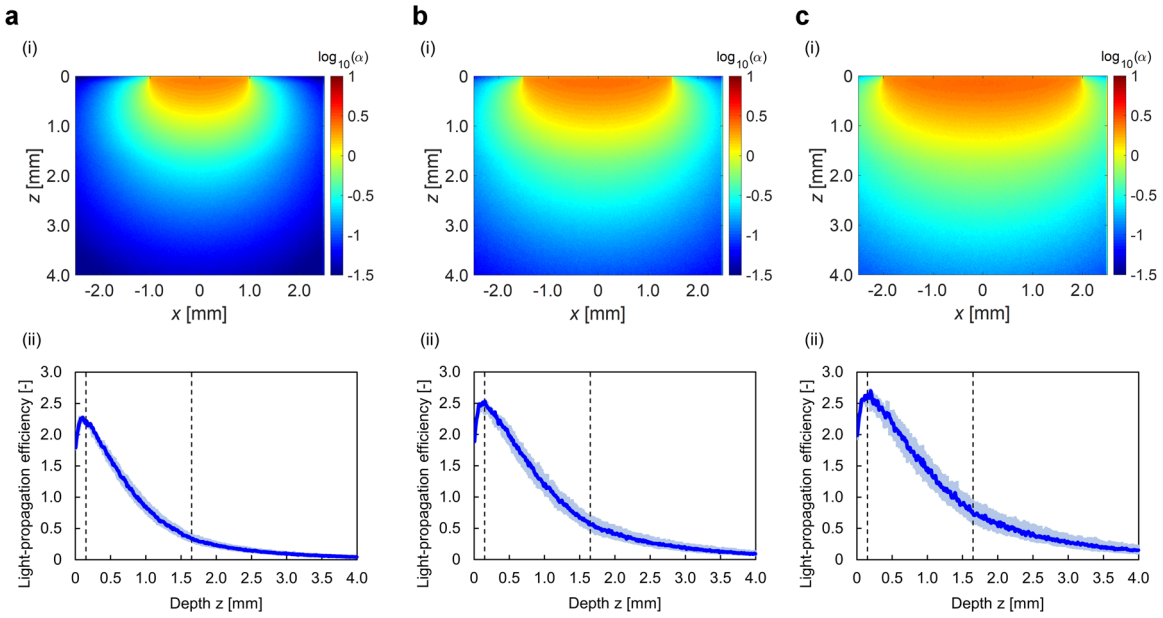

Fig. 4. Light-propagation efficiencies α produced through Monte Carlo simulation for spot sizes of (**a**) 2, (**b**) 3, and (**c**) 4 mm. (**i**) Spatial distributions on zx-plane with $y = 0$ and (**ii**) depth profiles along$z$-axis with $x = y = 0$. Broken lines at 0.15 and 1.65 mm exhibit boundaries between the epidermis and dermis and between the dermis and subcutaneous fat, respectively.

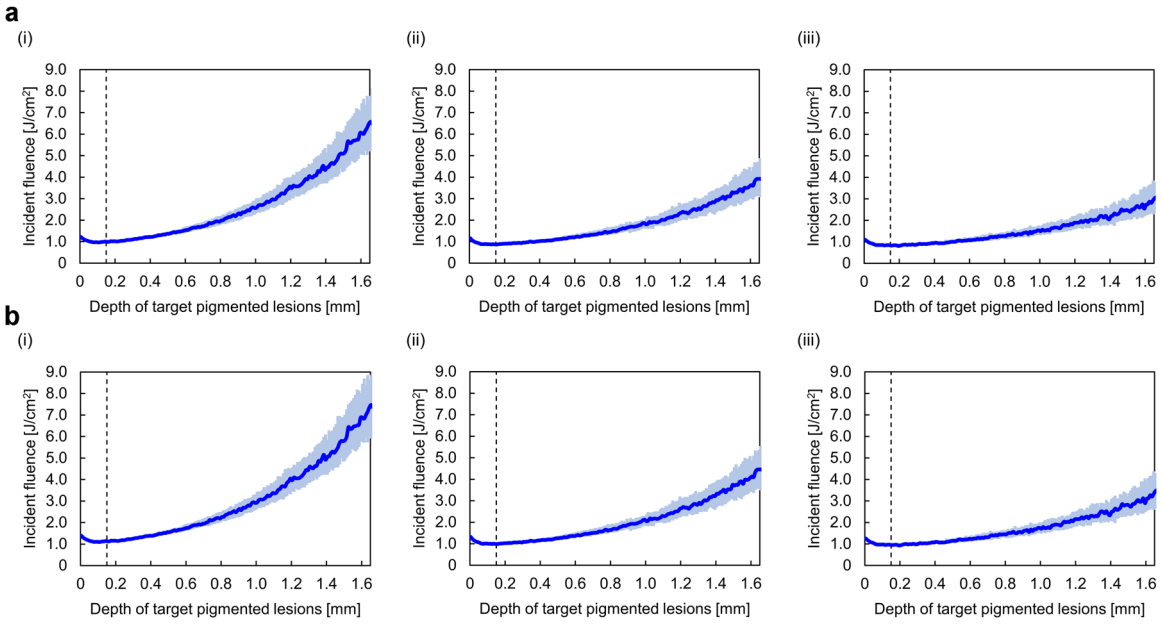

Fig. 5. Incident fluences F of (**a**) 550- and (**b**) 750-picosecond laser pulses for disruption of melanosomes with different depth distributions in skin tissue calculated at spot sizes of (**i**) 2, (**ii**) 3, and (**iii**) 4 mm. Broken line at 0.15 mm exhibits boundaries between the epidermis and dermis. The depth range of subcutaneous fat was not shown since pigmented skin lesions are located in the epidermis/dermis.

melanosomes are deeply distributed owing to the deviation of α. Because α increases near the dermal-epidermal junction, the incident fluences are found to decrease at its depth. In the incident fluences for the disruption of melanosomes distributed between the epidermis and lower dermis, differences of 5.3, 2.8, and 1.8 J/cm^2 for a 550-picosecond laser pulse and 6.0, 3.1, and 2.1 J/cm^2 for a 750-picosecond laser pulse occurred at spot sizes of 2, 3, and 4 mm, respectively.

DISCUSSION

The threshold fluences of the picosecond laser pulses are one-order-of-magnitude larger than the values of 532-nm nanosecond laser pulses for transient microbubble formation at a melanosome surface for selective retina treatment [12,16]. Neumann and Brinkmann [12] observed no hysteresis of the thresholds during repeated irradiations or morphological alterations of the melanosomes by optical microscopy after irradiation near the threshold. In comparison, our experiment used a different laser wavelength of 755 nm and determined the threshold fluences for the different selective responses, that is, melanosome disruption, which causes differences between our values and those previously reported. Glickman et al. [32] predicted the threshold fluence for melanosome disruption as 153.6 mJ/cm^2 when 10-nanosecond laser pulses at a wavelength of 532 nm were irradiated approximately 1800 times at 10 Hz. Our threshold fluences are larger than the reported values because they show those required for a melanosome disruption by a single pulse shot and without multiple irradiations.

The threshold fluences of 550- and 750-picosecond laser pulses were determined by evaluating the relationships between the irradiated fluences and the mean particle sizes resulting from the DLS analysis, and confirming their disruption when the mean particle sizes changed significantly using SEM. The decrease in the sizes of the disrupted melanosomes in the DLS analysis was consistent with the results of the SEM observation. Almost no differences occurred between these threshold fluences because both laser pulses meet the thermal confinement condition of melanosomes. Because the output stability of the picosecond laser fluences is ±20%, the threshold fluences might vary within that range. The effect of the difference in the unirradiated melanosome sizes on the thresholds is negligible (Fig. 2). This is because the absorbed laser energy density does not depend on the melanosome sizes, and the thermal relaxation time of the melanosomes is much smaller than the picosecond laser pulse widths, and thus the laser pulses satisfy the thermal confinement condition of the melanosomes regardless of the individual differences in the melanosome sizes. In Figure 2, there is almost no variation in the mean particle sizes of melanosomes irradiated above the threshold fluences. When the mean particle sizes irradiated at or above the thresholds are compared with those irradiated with the maximum fluences (5.25 and 5.26 J/cm^2 for 550- and 750-picosecond laser pulses, respectively), the differences were not significant for irradiations above 2.19 and 2.83 J/cm^2 for 550- and 750-picosecond laser pulses, respectively. This comparison implies that irradiation at a larger fluence has almost no effect on melanosome disruption.

The temperature rise needed for explosive vaporization is reasonably similar between porcine RPE melanosomes ($136 \pm 23°C$) [12] and human cutaneous melanosomes ($112 \pm 7°C$) [10] and is calculated from the irradiated fluence and absorption coefficients of melanosomes. The absorption coefficient of porcine RPE melanosomes was reported to be larger than that of human cutaneous melanosomes [10,12], which might affect the threshold fluences. Herein, picosecond laser pulses irradiated the melanosomes suspended in distilled water. From a thermal perspective, the interaction between the absorbing melanosomes and their surroundings are similar to actual skin because there is little difference in thermal diffusivity between the water and skin [12,33].

We calculated the incident fluences of picosecond laser pulses for disruption of the melanosomes at different skin-tissue depths using the threshold fluences obtained and a Monte Carlo simulation. The measured power density of the beam profile varied within the range of −20% to +30% from the averaged value. The beam profiles were uniform in the numerical simulations. When the power density of the uniform beam profiles varied within the same range, the calculated light distributions of skin tissue decreased by 20% for the minimum power density and increased by 30% for the maximum power density. Therefore, the calculated fluences varied within the range of −20% at minimum to +30% at maximum.

The simulation results were consistent with those reported for picosecond laser treatment of dermal pigmented lesions using the same laser device as in our experiment [34-36]. Clinical studies reported that patients with Fitzpatrick skin type III or IV suffering from nevus of Ota, Hori's macules, or ectopic Mongolian spots obtained good results without any complications through picosecond laser irradiation at a pulse width of 750 picoseconds, fluences of 1.59–5.26 J/cm^2, and spot sizes of 2.2–4.0 mm. The irradiated fluences for spot sizes of 3 and 4 mm were within the range of the incident fluences when the target melanosomes were distributed in the dermis. The simulation results revealed that the incident fluences needed for the disruption of melanosomes in skin tissues differ when the melanosomes are located in the epidermis and lower dermis, and the larger the spot size, the lower the incident fluence required to disrupt melanosomes in the deeper skin tissue (Fig. 5). These results have an important clinical implication in demonstrating that the appropriate choice of irradiation parameters is dependent on the pigmented lesion depth. In a clinical study of 755-nm picosecond laser treatment of epidermal pigmented lesions in Asians, a fluence of 3.5 J/cm^2 gave rise to marginal hyperpigmentation [37]. By contrast, our results indicate that a fluence of 1 J/cm^2 of picosecond laser pulses might be able to treat epidermal pigmented lesions with less damage to the surrounding tissues. Considering that our calculation used optical properties for Asian skin tissue, differences in skin type can influence the incident fluences obtained. The evaluations will compare the incident fluences calculated using the values for Caucasian and African skin tissues [5]. Figure 5 also shows a slight decrease in the incident fluences when the target melanosomes are around the dermal-epidermal junction. Because a laser wavelength of 755 nm, employed for picosecond laser devices, penetrates deeply into the skin

tissue [5] and has a large ratio of optical absorption by melanin relative to hemoglobin [38], the laser light is suitable for dermal pigmented lesion treatment [39-41]. The simulation results suggest that even if the appropriate incident fluences for disruption of melanosomes in the dermis layer are chosen, unavoidable injury at the junction may occur, often involving postinflammatory hyperpigmentation or hypopigmentation [36,42]. The design of a novel optical delivery system that allows a sufficient quantity of laser energy to reach the deep layer of skin tissue while reducing damage to the surface layer is required [43].

When the short-pulsed laser energy is directed at pigmented skin lesions, the therapeutic endpoint is usually immediate whitening, corresponding to increases in optical scattering with vacuolization of the melanosomes [3,4,44,45]. However, Ohshiro et al. [36] reported that patients with dermal pigmented lesions obtained successful lightning without immediate whitening in 12 of 16 treatments, implying that immediate whitening is not needed to achieve clinical clearance in picosecond laser treatments. Furthermore, immediate whitening can also occur in melanosomes in normal tissues that are distributed above pigmented lesions, which makes distinguishing them from melanosomes in pigmented lesions difficult. Therefore, it is difficult to determine through a visual assessment if the desired energy is delivered to the target lesions. These contradictions suggest the necessary quantitative evaluation of irradiation conditions for pigmented lesion treatment based on the threshold fluences for melanosome disruption and light-propagation analysis. The calculated incident fluences can provide fundamental knowledge to establish quantitative indexes for choosing the irradiation endpoint of picosecond laser pulses. The validation of our simulation results will lead to improved picosecond laser irradiation approaches for pigmented skin lesion treatment.

CONCLUSION

Threshold fluences of 550- and 750-picosecond laser pulses for therapeutic use causing melanosome disruption were determined to be 2.19 and 2.49 J/cm^2, respectively. Light transport simulations revealed that appropriate incident fluences of picosecond laser pulses for the disruption of melanosomes in skin tissue are dependent on their depth distribution. Choosing a larger laser spot size can disrupt the melanosomes in the deeper part of the skin tissue with minimal damage to the surrounding tissues because a lesser incident fluence is necessary. An incident fluence analysis based on the melanosome disruption thresholds provides information determining the irradiation endpoint for picosecond laser treatment of pigmented skin lesions. Validation is needed to establish quantitative indexes and choose appropriate irradiation parameters for picosecond laser treatment using novel therapeutic laser devices.

ACKNOWLEDGMENTS

The authors appreciate the technical support of the picosecond laser device provided by Cynosure LLC. and the cooperation of Prof. Satoshi Seino and Prof. Yoko Akiyama of Osaka University during the experiment using the particle size analyzer. This work was supported by the Japan Society for the Promotion of Science KAKENHI (Grant Number 19K22966).

REFERENCES

1. Anderson RR, Parrish JA. Selective photothermolysis: Precise microsurgery by selective absorption of pulsed radiation. Science 1983;220(4596):524–527. https://doi.org/10.1126/science.6836297
2. Lee HC, Childs J, Chung HJ, et al. Pattern analysis of 532- and 1,064-nm picosecond-domain laser-induced immediate tissue reactions in *ex vivo* pigmented micropig skin. Sci Rep 2019;9(1):1–10. https://doi.org/10.1038/s41598-019-41021-7
3. Polla LL, Margolis RJ, Dover JS, et al. Melanosomes are a primary target of *Q*-switched ruby laser irradiation in guinea pig skin. J Invest Dermatol 1987;89(3):281–286. https://doi.org/10.1111/1523-1747.ep12471397
4. Anderson RR, Margolis RJ, Watanabe S, et al. Selective photothermolysis of cutaneous pigmentation by *Q*-switched Nd:YAG laser pulses at 1064, 532, and 355 nm. J Invest Dermatol 1989;93(1):28–32. https://doi.org/10.1111/1523-1747.ep12277339
5. Shimojo Y, Nishimura T, Hazama H, Ozawa T, Awazu K. Measurement of absorption and reduced scattering coefficients in Asian human epidermis, dermis, and subcutaneous fat tissues in the 400- to 1100-nm wavelength range for optical penetration depth and energy deposition analysis. J Biomed Opt 2020;25(4):045002. https://doi.org/10.1117/1.jbo.25.4.045002
6. Salomatina E, Jiang B, Novak J, Yaroslavsky AN. Optical properties of normal and cancerous human skin in the visible and near-infrared spectral range. J Biomed Opt 2006;11(6):064026. https://doi.org/10.1117/1.2398928
7. Watanabe S, Takahashi H. Treatment of nevus of Ota with the *Q*-switched ruby laser. N Engl J Med 1994;331(26):1745–1750.
8. Negishi K, Akita H, Matsunaga Y. Prospective study of removing solar lentigines in Asians using a novel dual-wavelength and dual-pulse width picosecond laser. Lasers Surg Med 2018;50(8):851–858. https://doi.org/10.1002/lsm.22820
9. Kung KY, Shek SYN, Yeung CK, Chan HHL. Evaluation of the safety and efficacy of the dual wavelength picosecond laser for the treatment of benign pigmented lesions in Asians. Lasers Surg Med 2019;51(1):14–22. https://doi.org/10.1002/lsm.23028
10. Jacques SL, McAuliffe DJ. The melanosome: Threshold temperature for explosive vaporization and internal absorption coefficient during pulsed laser irradiation. Photochem Photobiol 1991;53(6):769–775. https://doi.org/10.1111/j.1751-1097.1991.tb09891.x
11. Watanabe S, Anderson RR, Brorson S, et al. Comparative studies of femtosecond to microsecond laser pulses on selective pigmented cell injury in skin. Photochem Photobiol 1991;53(6):757–762. https://doi.org/10.1111/j.1751-1097.1991.tb09889.x
12. Neumann J, Brinkmann R. Boiling nucleation on melanosomes and microbeads transiently heated by nanosecond and microsecond laser pulses. J Biomed Opt 2005;10(2):024001. https://doi.org/10.1117/1.1896969
13. Lee H, Alt C, Pitsillides CM, Lin CP. Optical detection of intracellular cavitation during selective laser targeting of the retinal pigment epithelium: Dependence of cell death mechanism on pulse duration. J Biomed Opt 2007;12(6):064034. https://doi.org/10.1117/1.2804078

14. Schmidt MS, Kennedy PK, Vincelette RL, et al. Trends in melanosome microcavitation thresholds for nanosecond pulse exposures in the near infrared. J Biomed Opt 2014;19(3):035003. https://doi.org/10.1117/1.jbo.19.3.035003
15. Schmidt MS, Kennedy PK, Noojin GD, Thomas RJ, Rockwell BA. Temperature dependence of nanosecond laser pulses thresholds of melanosome and microsphere microcavitation. J Biomed Opt 2016;21(1):015013. https://doi.org/10.1117/1.JBO.21.1.015013
16. Deladurantaye P, Méthot S, Mermut O, Galarneau P, Rochette PJ. Potential of sub-microsecond laser pulse shaping for controlling microcavitation in selective retinal therapies. Biomed Opt Express 2020;11(1):109. https://doi.org/10.1364/boe.11.000109
17. Luecking M, Brinkmann R, Ramos S, Stork W, Heussner N. Capabilities and limitations of a new thermal finite volume model for the evaluation of laser-induced thermo-mechanical retinal damage. Comput Biol Med 2020;122:103835. https://doi.org/10.1016/j.compbiomed.2020.103835
18. Flock ST, Patterson MS, Wilson BC, Wyman DR. Monte Carlo modeling of light propagation in highly scattering tissue. I. Model predictions and comparison with diffusion theory. IEEE Trans Biomed Eng 1989;36(12):1162–1168. https://doi.org/10.1109/TBME.1989.1173624
19. Meglinski IV, Matcher SJ. Computer simulation of the skin reflectance spectra. Comput Methods Programs Biomed 2003;70(2):179–186. https://doi.org/10.1016/S0169-2607(02)00099-8
20. Zhu C, Liu Q. Review of Monte Carlo modeling of light transport in tissues. J Biomed Opt 2013;18(5):050902. https://doi.org/10.1117/1.jbo.18.5.050902
21. Periyasamy V, Pramanik M. Advances in Monte Carlo simulation for light propagation in tissue. IEEE Rev Biomed Eng 2017;10:122–135. https://doi.org/10.1109/RBME.2017.2739801
22. Wasilewska M, Adamczyk Z, Jachimska B. Structure of fibrinogen in electrolyte solutions derived from dynamic light scattering (DLS) and viscosity measurements. Langmuir 2009;25(6):3698–3704. https://doi.org/10.1021/la803662a
23. Stetefeld J, McKenna SA, Patel TR. Dynamic light scattering: A practical guide and applications in biomedical sciences. Biophys Rev. 2016;8(4):409–427. https://doi.org/10.1007/s12551-016-0218-6
24. Song W, Zhang L, Ness S, Yi J. Wavelength-dependent optical properties of melanosomes in retinal pigmented epithelium and their changes with melanin bleaching: A numerical study. Biomed Opt Express 2017;8(9):3966–3980. https://doi.org/10.1364/boe.8.003966
25. Jacques SL. Coupling 3D Monte Carlo light transport in optically heterogeneous tissues to photoacoustic signal generation. Photoacoustics 2014;2(4):137–142. https://doi.org/10.1016/j.pacs.2014.09.001
26. Handapangoda CC, Premaratne M, Yeo L, Friend J. Laguerre Runge-Kutta-Fehlberg method for simulating laser pulse propagation in biological tissue. IEEE J Sel Top Quantum Electron 2008;14(1):105–112. https://doi.org/10.1109/JSTQE.2007.913971
27. Mitra K, Kumar S. Development and comparison of models for light-pulse transport through scattering–absorbing media. Appl Opt 1999;38(1):188–196. https://doi.org/10.1364/ao.38.000188
28. Suthamjariya K, Farinelli WA, Koh W, Anderson RR. Mechanisms of microvascular response to laser pulses. J Invest Dermatol 2004;122(2):518–525. https://doi.org/10.1046/j.0022-202X.2004.22241.x
29. Ekici O, Harrison RK, Durr NJ, et al. Thermal analysis of gold nanorods heated with femtosecond laser pulses. J Phys D Appl Phys 2008;41(18):185501. https://doi.org/10.1088/0022-3727/41/18/185501
30. Varghese B, Bonito V, Jurna M, et al. Influence of absorption induced thermal initiation pathway on irradiance threshold for laser induced breakdown. Biomed Opt Express 2015;6(4):1234–1240. https://doi.org/10.1364/boe.6.001234
31. Shimojo Y, Nishimura T, Hazama H, Ito N, Awazu K. Picosecond laser-induced photothermal skin damage evaluation by computational clinical trial. Laser Ther 2020;29(1):61–72. https://doi.org/10.5978/islsm.20-OR-08
32. Glickman RD, Jacques SL, Schwartz JA, et al. Photodisruption increases the free-radical reactivity of melanosomes isolated from retinal pigment epithelium. Proc SPIE 1996;2681:460–467. https://doi.org/10.1117/12.239607
33. Duck FA. Thermal Properties of Tissue. Physical Properties of Tissues: A Comprehensive Reference Book. London: Academic Press; 1990. pp 9–42. https://doi.org/10.1016/B978-0-12-222800-1.50006-1
34. Chesnut C, Diehl J, Lask G. Treatment of nevus of Ota with a picosecond 755-nm alexandrite laser. Dermatol Surg 2015;41(4):508–510. https://doi.org/10.1097/DSS.0000000000000326
35. Chan JC, Shek SY, Kono T, Yeung CK, Chan HH. A retrospective analysis on the management of pigmented lesions using a picosecond 755-nm alexandrite laser in Asians. Lasers Surg Med 2016;48(1):23–29. https://doi.org/10.1002/lsm.22443.
36. Ohshiro T, Ohshiro T, Sasaki K, Kishi K. Picosecond pulse duration laser treatment for dermal melanocytosis in Asians: A retrospective review. Laser Ther 2016;25(2):99–104. https://doi.org/10.5978/islsm.16-OR-07
37. Kasai K. Picosecond laser treatment for tattoos and benign cutaneous pigmented lesions (Secondary publication). Laser Ther 2017;26(4):274–281. https://doi.org/10.5978/islsm.17-RE-02
38. Jacques SL. Skin optics. Oregon Med Laser Cent News. https://omlc.org/news/jan98/skinoptics.html. Accessed August 17, 2020.
39. Chan HH, Leung RSC, Ying SY, et al. A retrospective analysis of complications in the treatment of nevus of Ota with the *Q*-switched alexandrite and *Q*-switched Nd:YAG lasers. Dermatol Surg 2000;26(11):1000–1006. https://doi.org/10.1046/j.1524-4725.2000.0260111000.x
40. Ge Y, Yang Y, Guo L, et al. Comparison of a picosecond alexandrite laser versus a *Q*-switched alexandrite laser for the treatment of nevus of Ota: A randomized, split-lesion, controlled trial. J Am Acad Dermatol 2020;83(2):397–403. https://doi.org/10.1016/j.jaad.2019.03.016
41. Hu S, Yang CS, Chang SL, Huang YL, Lin YF, Lee MC. Efficacy and safety of the picosecond 755-nm alexandrite laser for treatment of dermal pigmentation in Asians—A retrospective study. Lasers Med Sci 2020;35(6):1377–1383. https://doi.org/10.1007/s10103-020-02959-7
42. Sakio R, Ohshiro T, Sasaki K, Ohshiro T. Usefulness of picosecond pulse alexandrite laser treatment for nevus of Ota. Laser Ther 2018;27(4):251–255. https://doi.org/10.5978/islsm.27_18-OR-22
43. Burns JM, Jia W, Nelson JS, Majaron B, Anvari B. Photothermal treatment of port-wine stains using erythrocyte-derived particles doped with indocyanine green: A theoretical study. J Biomed Opt. 2018;23(12):121616. https://doi.org/10.1117/1.jbo.23.12.121616
44. Taylor CR, Anderson RR. Treatment of benign pigmented epidermal lesions by *Q*-switched ruby laser. Int J Dermatol 1993;32(12):908–912. https://doi.org/10.1111/j.1365-4362.1993.tb01417.x
45. Wanner M, Sakamoto FH, Avram MM, et al. Immediate skin responses to laser and light treatments therapeutic endpoints: How to obtain efficacy. J Am Acad Dermatol 2016;74(5):821–833. https://doi.org/10.1016/j.jaad.2015.06.02